Frank's constant in the hexatic phase

P. Keim,[1] G. Maret,[2] and H. H. von Grünberg[1]

[1]*Universität Graz, 8010 Graz, Austria*
[2]*Universität Konstanz, 78457 Konstanz, Germany*

Using videomicroscopy data of a two-dimensional colloidal system the bond-order correlation function G_6 is calculated and used to determine both the orientational correlation length ξ_6 in the liquid phase and the modulus of orientational stiffness, Frank's constant F_A, in the hexatic phase. The latter is an anisotropic fluid phase between the crystalline and the isotropic liquid phase. F_A is found to be finite within the hexatic phase, takes the value $72/\pi$ at the hexatic↔isotropic liquid phase transition, and diverges at the hexatic↔crystal transition as predicted by the Kosterlitz-Thouless-Halperin-Nelson-Young theory. This is a quantitative test of the mechanism of breaking the orientational symmetry by disclination unbinding.

I. INTRODUCTION

The theory of melting in two dimensions (2D), developed by Kosterlitz, Thouless, Halperin, Nelson, and Young (KTHNY) has been a matter of debate over decades. In a 2D crystal, the density-density correlation function is an algebraically decaying function and is not given by a set of δ peaks as in a 3D crystal. This decay behavior indicates a quasi-long-range translational order and is ultimately due to long-wavelength fluctuations [1]. In the fluid phase then the translational symmetry is completely destroyed so that the translational correlation function decays exponentially. This implies a vanishing of the shear modulus.

According to Kosterlitz and Thouless, the phase transition from the solid to the fluid phase is driven by the dissociation of thermally activated dislocation pairs [2,3]. Nelson and Halperin then showed that the fluid phase above the melting temperature T_m still exhibits quasi-long-range orientational order with a sixfold director [4,5]. This anisotropic fluid phase is called hexatic. The orientational correlation function of the hexatic phase decays algebraically and is associated with a nonvanishing elastic modulus of the orientational stiffness. This modulus is Frank's constant F_A.

At a temperature $T_i > T_m$ the orientational symmetry changes again which can be seen from the orientational correlation function switching from an algebraic to an exponential decay. According to the KTHNY theory, this change is the consequence of the emergence of a second class of topological defects, the disclinations, which occur as a result of the dissociation of some of the dislocations. Finally, above T_i the fluid shows ordinary short-range rotational and positional order as it is characteristic of an isotropic liquid.

Following an argument given in [2,5], T_m and T_i can be estimated using the defect interaction Hamiltonian H_d between a pair of disclinations (d=disc) and a pair of dislocations (d=disl) which for both defect pairs and at large distances goes like

$$\beta H_d = c_d \ln r/r_c, \tag{1}$$

with $\beta = 1/k_B T$, r_c being the defect-core radius, and the dimensionless strength parameter c_d depending on the defect

type. Defect dissociation is completed at a temperature where the thermally averaged pair distance

$$\langle r^2 \rangle = \frac{\int d^2 r r^2 e^{-\beta H_d}}{\int d^2 r e^{-\beta H_d}} = \frac{2 - c_d}{4 - c_d} r_c^2 \tag{2}$$

diverges which is obviously the case if $c_d \to 4$. Inserting into $c_d \to 4$ the respective expressions for c_d for d=disc and d=disl, we are led to two unbinding conditions which are

$$\lim_{T \to T_m^-} \beta \mathcal{K}(T) a_0^2 = 16\pi \tag{3}$$

for dislocation-pair unbinding and

$$\lim_{T \to T_i^-} \beta F_A(T) = 72/\pi \tag{4}$$

for disclination-pair unbinding. Here, β is $1/k_B T$, a_0 is the lattice constant, and $\mathcal{K}$ stands for the Young's modulus of the crystal. These relations—connecting the two transition temperatures T_i and T_m with macroscopic quantities characterizing the elastic properties of the system—reflect a universal behavior of 2D systems independent of microscopic interactions.

In this article we study the temperature dependence of Frank's constant of a 2D system in the hexatic phase. We first determine the hexatic→isotropic fluid transition temperature T_i and then check if Frank's constant takes the value $72/\pi$ at T_i, thus testing the KTHNY theory and its prediction that disclination unbinding occurs at T_i. In addition, we analyze the divergence behavior of the orientational correlation length at T_i and of Frank's constant at T_m. To learn more about the order of the transitions, we furthermore study the probability distribution of the local bond order parameter.

Different theoretical approaches invoking grain boundary induced melting [6,7] or condensation of geometrical defects [8,9] suggest one first-order transition. However, some simulations for Lennard-Jones systems indicate the hexatic phase to be metastable [10,11]. The transition in hard-core systems seems to be first order [12] probably due to finite-size effects [13]. Simulations with long-range dipole-dipole interaction clearly show second-order behavior [14]. Experimental evidence for the hexatic phase has been demonstrated for col-
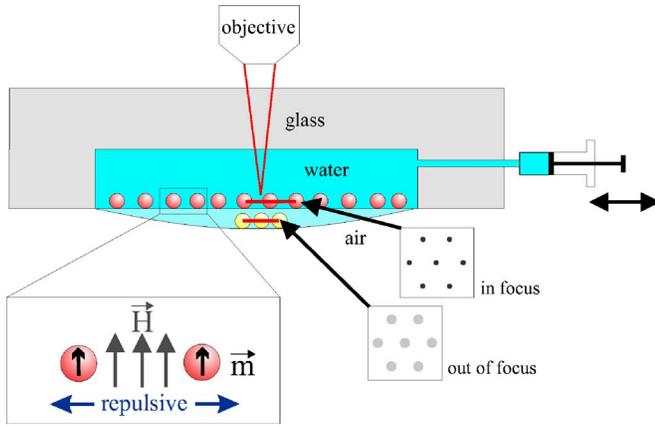
FIG. 1. (Color online) Superparamagnetic colloids confined at a water/air interface due to gravity (side view). A magnetic field $\vec{H}$ perpendicular to the interface induces a magnetic moment $\vec{m}$ leading to a repulsive interaction. The curvature of the interface is regulated by the volume of the droplet using a computer controlled syringe. The set point is the projected size of the colloids giving information about the position of the interface with respect to the focal plane. Colloids appear smallest when in focus and larger out of focus.

loidal systems [15–20], in block copolymer films [21,22], as well as for magnetic bubble arrays and macroscopic granular or atomic systems [23–27]. Still the order of the transitions is seen to be inconsistent. The observation of a phase equilibrium isotropic/hexatic [18,22] and hexatic/crystalline [18] indicates two first-order transitions. In our system we find two continuous transitions.

II. EXPERIMENTAL SETUP

The experimental setup is essentially the same as in [28]. Spherical and superparamagnetic colloids (diameter $d = 4.5$ μm) are confined by gravity to a water/air interface formed by a water drop suspended by surface tension in a top sealed cylindrical hole (8 mm diameter) of a glass plate; see Fig. 1. A magnetic field $\vec{H}$ is applied perpendicular to the air/water interface inducing a magnetic moment $\vec{M} = \chi \vec{H}$ in each particle. This leads to a repulsive dipole-dipole pair-interaction E_{magn} with the dimensionless interaction strength given by

$$\Gamma = \frac{E_{magn}}{k_B T} = \frac{\mu_0}{4\pi} \frac{\chi^2 \vec{H}^2 (\pi\rho)^{3/2}}{k_B T} \propto \frac{1}{T_{sys}}. \tag{5}$$

Here ρ is the 2D particle density and the average particle distance is $a = 1/\sqrt{\rho}$. The interaction strength can be externally controlled by means of the magnetic field H; it can be interpreted as an inverse temperature and controls the phase behavior of the system.

The ensemble of particles is visualized with video microscopy from above and the signal of a charge coupled device (CCD) 8-bit gray-scale camera is analyzed on a computer. The field of view has a size of 835×620 μm^2 containing typically up to 3×10^3 particles, whereas the whole sample contains about up to 3×10^5 particles. In order to get the size, number, and positions of the colloids the image is binarized: The software recognizes areas of connected pixels with respect to the background and the amount of pixels of each connected area gives the size of the colloids and the barycenter gives its position. The average projected size of the colloids contains information about the vertical position of the interface relative to the focus of the camera. If the camera is moved in a vertical direction, particle images are smallest in focus and larger out of focus. This information is used to maintain a flat water surface by compensating for the loss of water due to evaporation: A computer-controlled syringe driven by a microstage controls the volume of the droplet and thereby the curvature of the interface. An active regulation of the vertical camera position is overlayed to get a completely flat surface. The set point is the number of particles in the field of view chosen to reach a homogeneous number density profile throughout the whole sample. I.e., if the interface is convex, particle density will rise in the middle of the sample due to gravity. Then the camera is lifted by a microstage; the interface gets out of focus which is compensated by the regulation of the syringe and vice versa. In this way fluctuations around the set point of particle number are suppressed below 1% and the largest observed particle-density gradient in the horizontal plane is less than 1%. The latter is done by the variation of the inclination of the whole experimental setup. The inclination is also controlled actively by microstages with a resolution in the range of $\alpha \approx 5$ μrad. After several weeks of adjusting and equilibration this provides best equilibrium conditions for long time stability. During data acquisition the images are analyzed with a frame rate of 250 ms and the coordinates of all particles are recorded for every time step containing the whole phase space information. The thermal activated out-of-plane motion of the colloids is in the range of a few tenths of a nanometer, so the ensemble is supposed to be an ideal two-dimensional system.

III. RESULTS

To set the stage we first visualize in Fig. 2 the three phases and their symmetries by plotting the structure factor

$$S(\vec{q}) = \frac{1}{N} \left\langle \sum_{\alpha,\alpha'} e^{-i\vec{q}\cdot(\vec{r}_\alpha - \vec{r}_{\alpha'})} \right\rangle, \tag{6}$$

as calculated from the positional data of the colloids for three different temperatures. Here, α, α' run over all N particles in the field of view and a time average is taken over 700 configurations. In the liquid phase, concentric rings appear having radii that can be connected to typical interparticle distances. The hexatic phase, on the other hand, is characterized by six segments of a ring which arise due to the quasi-long-range orientational order of the sixfold director [29]. In the crystalline phase the Bragg peaks of finite width show up [1], reflecting the quasi-long-range character of the translational order in two dimensions.
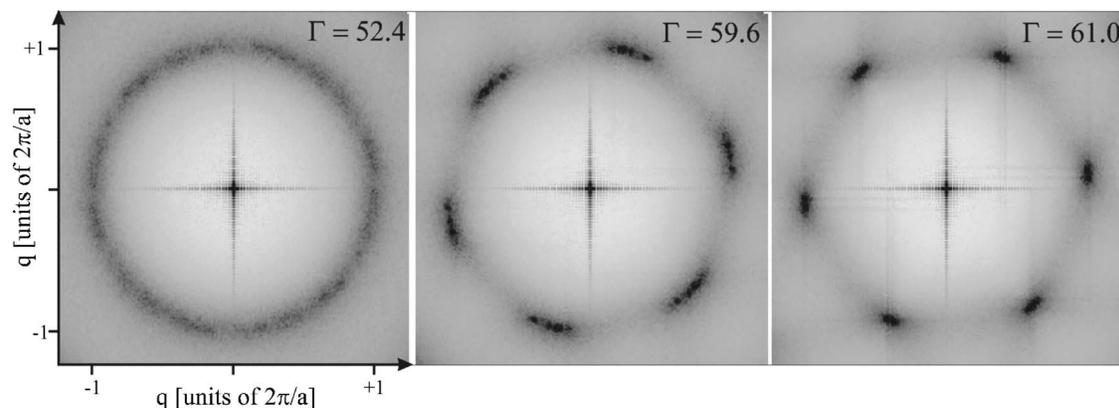
FIG. 2. Structure factor $S(\vec{q})$ of our colloidal system at three different inverse temperatures Γ corresponding to the isotropic liquid phase ($\Gamma=52.4$), the hexatic phase ($\Gamma=59.6$), and the crystalline phase ($\Gamma=61.0$). The central cross is an artifact of the Fourier transformation arising from the rectangle field of view.

A. Orientational symmetry

To quantify the sixfold orientational symmetry the bond-order correlation function

$$G_6(r) = \langle \psi(\vec{r})\psi^*(\vec{0}) \rangle \tag{7}$$

is calculated with $\psi(\vec{r}) = \psi_k = \frac{1}{N_j}\Sigma_j e^{i6\theta_{jk}}$. Here the sum runs over the N_j next neighbors of the particle k at position $\vec{r}$ and θ_{jk} is the angle between a fixed reference axis and the bond of the particle k and its neighbor j. The average is not only the ensemble average which is taken over all $N(N-1)/2$ particle-pair distances for each configuration (resolution $dr = 100$ nm) but also the time average over 70 statistically independent configurations. KTHNY theory predicts that

$$\lim_{r \to \infty} G_6(r) \neq 0 \quad \text{crystal: long-range order,}$$

$$G_6(r) \sim r^{-\eta_6} \quad \text{hexatic: quasi-long-range order,}$$

$$G_6(r) \sim e^{-r/\xi_6} \quad \text{isotropic: short-range order.}$$

In the hexatic phase $\eta_6 < 1/4$ and takes the value $1/4$ right at $T=T_i$. All three regimes can be easily distinguished in Fig. 3

showing $G_6(r)$ for a few representative temperatures. Note that $G_6(0)$ is not normalized to 1. In the crystalline phase $\lim_{r \to \infty} G_6(r)$ is connected to the shear modulus [5], so decreasing values of this limes for decreasing interaction strength reflect the softening of the crystal due to phonons and thermally activated but bound (virtual) dislocation pairs.

B. Correlation length

We next fit $G_6(r)$ to $r^{-\eta_6}$ and e^{-r/ξ_6} to extract η_6 and ξ_6 in the isotropic fluid and the hexatic phase. The fits are performed for radii $r/a \in \{0...20\}$ [30]. To check for the characteristics of the orientational correlation function, the ratio of the reduced chi-square χ^2 goodness-of-fit statistic of the algebraic (χ^2_{alg}) and exponential (χ^2_{exp}) fit is shown in Fig. 4 as a function of Γ for three different measurements. For melting, a crystal free of dislocations was grown at high Γ and then Γ was reduced in small steps. For each temperature step the system was equilibrated $1/2$ h before data acquisition started. This was done at different densities: melt_1 with average particle distance of $a=11.8$ μm and melt_2 with a
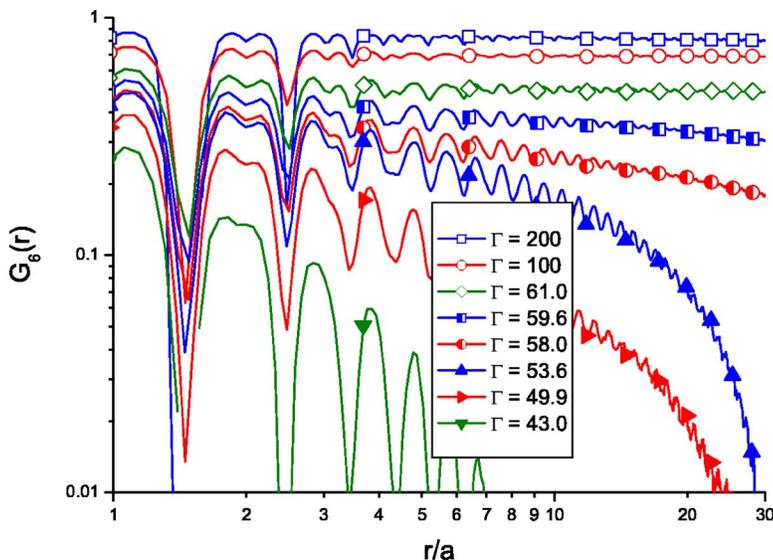

FIG. 3. (Color online) Orientational correlation function $G_6(r)$ as a function of the inverse temperature Γ in a log-log plot. From top to bottom: three curves for the crystalline phase showing the long-range orientational order $[\lim_{r \to \infty} G_6(r) \neq 0]$, two curves showing the quasi-long-range order of the hexatic phase $[G_6(r) \sim r^{-\eta_6(\Gamma)}]$, and three curves showing the short-range order typical of the isotropic liquid $[G_6(r) \sim e^{-r/\xi_6(\Gamma)}]$.
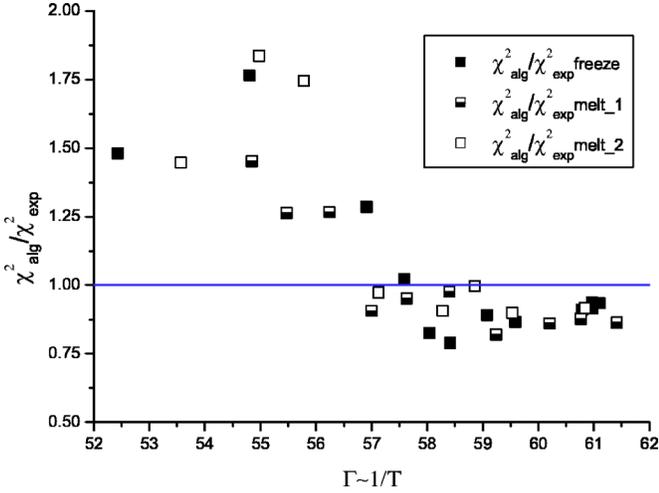
FIG. 4. (Color online) Quantitative test for the long-distance behavior of $G_6(r)$. For $\chi^2_{alg}/\chi^2_{exp} < 1$ the algebraic decay fits better.

$= 14.8$ μm containing 3200 and 2000 particles, respectively, in the field of view. The measurement denoted "freeze" in Fig. 4 ($a = 11.8$ μm) started in the isotropic liquid phase and Γ was increased with an equilibration time of 1 h between the steps. For $\chi^2_{alg}/\chi^2_{exp} > 1$ an exponential decay fits better than the algebraic and vice versa for $\chi^2_{alg}/\chi^2_{exp} < 1$. We observe in Fig. 4 that the change in the characteristic appears at $\Gamma_i = 57.5 \pm 0.5$. This value is the temperature of the hexatic $\leftrightarrow$ isotropic liquid transition.

In the vicinity of the phase transition, approaching Γ_i from the isotropic liquid the orientational correlation length ξ_6 should diverge as [5]

$$\xi_6(\Gamma) \sim \exp\left(\frac{b}{|1/\Gamma - 1/\Gamma_i|^\nu}\right), \qquad (8)$$

with b a constant and $\nu = 1/2$. This behavior is observed in Fig. 5(a). ξ_6 indeed increases dramatically near $\Gamma_i = 57.5 \pm 0.5$ irrespective of whether the system is heated or cooled. Before discussing this feature we first address the finite-size effect. To this end, we have computed $G_6(r)$ and ξ_6 for subsystems of different size, 720×515 μm^2, 615×405 μm^2, 505×300 μm^2, 400×190 μm^2, and 390×80 μm^2. The resulting data points are plotted as triangles in Fig. 5 and belong to the black solid squares which they converge to. No finite-size effect is found for $\Gamma < 56$, but a considerable one at $\Gamma = 56.9$ close to Γ_i where we obviously need the full field of view to capture the characteristic of the divergence. At $\Gamma = 58.0$ there is a huge finite-size effect indicating that ξ_6 is much larger than the field of view. However, inside the hexatic phase, ξ_6 is no longer well defined as the decay is algebraic. We fit our data to Eq. (8) in the range $49 < \Gamma < 57.5$ with Γ_i and b as fit parameters and find $\Gamma_i = 58.9 \pm 3.1$, a value which due to the finite-size effect is larger than Γ_i obtained from Fig. 4.

The exponent η_6 is related to Frank's constant F_A [5]:

$$\eta_6(\Gamma) = \frac{18 k_B T}{\pi F_A(\Gamma)}. \qquad (9)$$

So the critical exponent $\eta_6(\Gamma_i) = 1/4$ corresponds to $\beta F_A(\Gamma_i) = 72/\pi$ at the hexatic $\leftrightarrow$ liquid transition. This quan-
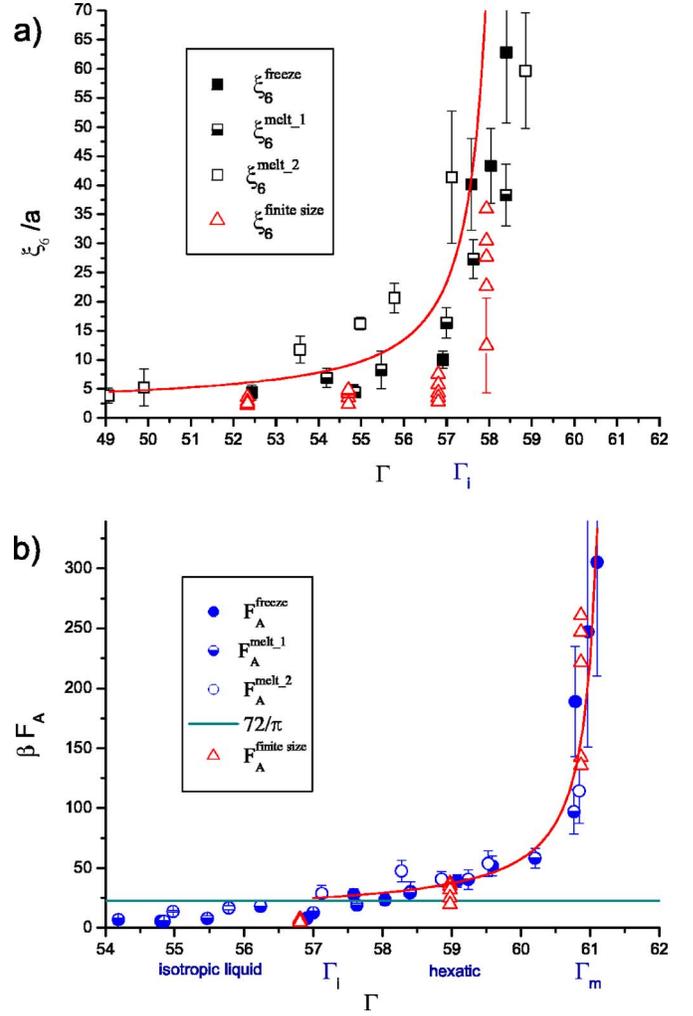

FIG. 5. (Color online) Correlation length ξ_6 (a) and Frank's constant F_A (b) as a function of the inverse temperature. ξ_6 diverges at Γ_i and F_A at Γ_m. In between the system shows hexatic symmetry. The solid lines are fits to Eqs. (8) and (10). Triangles are shifted by 0.1Γ for clarity.

tity is plotted in Fig. 5(b). Indeed, F_A crosses the value $72/\pi$ at $\Gamma_i = 57.5 \pm 0.5$ exactly at that temperature which in Fig. 4 has been independently determined to be the transition temperature T_i. For $\Gamma < \Gamma_i$, F_A should jump to zero which is not completely reproduced. We note that since η_6 is not well defined in the isotropic fluid, it becomes problematic to extract F_A from Eq. (9) below Γ_i. At Γ_m, at the hexatic $\rightarrow$ crystalline transition, F_A must diverge which indeed it does. This divergence can be identified with the divergence of the square of the translational correlation length ξ_+ [5]:

$$F_A(\Gamma)/k_B T \sim \xi_+^2 \sim \exp\left(\frac{2c}{|1/\Gamma - 1/\Gamma_m|^{\bar\nu}}\right), \qquad (10)$$

where c is again a constant and the theoretical value of the exponent is $\bar\nu = 0.369\,63$. Fitting the values of F_A to the expression in Eq. (10) in the range $57.5 < \Gamma < 61$ with Γ_m and c as fit parameters we obtain $\Gamma_m = 61.4 \pm 1.9$ as an upper threshold. Again triangles represent evaluation of our data in sub-
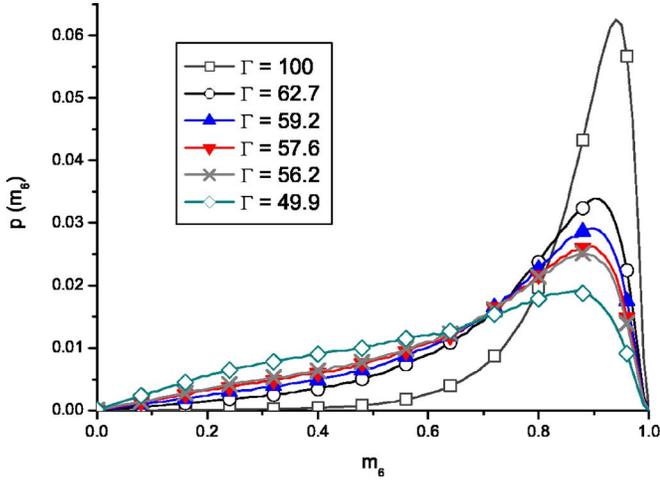
FIG. 6. (Color online) Probability distribution m_6 of the local bond order parameter: deep inside the crystalline phase (squares), crystalline phase close to Γ_m (circles), two curves for the hexatic phase (triangles), isotropic phase close to Γ_i (crosses), and deep in the isotropic phase (diamonds).

windows of variable size (same sizes as above). The finite-size effect for $\Gamma = 57.0$ is negligible. Close to Γ_m it increases but the values saturate for $\Gamma = 59.1$ and $\Gamma = 60.8$ and remain within the error bars for the largest subwindows. We do not find strong fluctuations of the correlation length near the transition points as observed in [22] where these fluctuations are interpreted as being a consequence of phase separation. Since the hexatic phase is a solid with respect to rotational forces, the fluctuations could possibly result also from the orientational polycrystallinity of the samples.

C. Local bond-order field

To get further insight into the local symmetry we focus on the magnitude of the local bond-order parameter,

$$m_{6_k} = |\psi_k|. \tag{11}$$

m_{6_k} can be considered as a measure quantifying the extent to which the bonds between particle k and its neighbors agree with the links between sites of a space-fixed hexagonal lattice. m_{6_k} is zero for perfect fivefold or sevenfold particles and one for perfect sixfold ones. Figure 6 shows the distribution of m_{6_k} for various temperatures, both close to and far away from the phase transitions. The well-pronounced maximum deep inside the crystalline phase for particles with sixfold symmetry decreases for decreasing Γ. This corresponds to

the increase of particles contributing to topological defects as determined by analysis of the nearest-neighbor statistics ($\sim 2\%$ at Γ_m and $\sim 10\%$ at Γ_i). An equally meaningful measure for quantifying the local symmetry is the magnitude of the projection of ψ_k onto the mean local orientation field,

$$n_{6_k} = \left| \psi_k^* \frac{1}{N_l} \sum_l \psi_l \right|, \tag{12}$$

where all particles with index l are neighbors of particle k. n_{6_k} takes also the second nearest neighbors into account and quantifies how good the orientation of particle k fits into the local hexagonal symmetry as defined by the orientation of its neighbor particles. Since it is a projection, $n_{6_k} \leq m_{6_k}$. And furthermore $n_{6_k} + m_{6_k} \leq 2$. Figure 7 shows the probability distribution in the m_6-n_6 plane for the same temperatures as in Fig. 6. In [31] areas of $m_6 + n_6 > 1$ (upper right corner) were used as empirical criteria for crystal-like particles. If one would expect phase separation as a sign for first-order transitions [18,22], a bimodal probability distribution for fluid-like and crystal-like particles should appear. This is definitely not the case here. No such bimodal distribution is observed; nor can we find any qualitative changes of the local bond-order field, neither above nor below Γ_i and Γ_m. This observation points to two continuous phase transitions.

IV. CONCLUSION

In conclusion, we have checked quantitatively the change of quasi-long-range to short-range orientational order and extracted the correlation length ξ_6 in the isotropic fluid and Frank's constant F_A in the hexatic phase from trajectories of a 2D colloidal system. We find a hexatic $\leftrightarrow$ isotropic liquid transition at $\Gamma_i = 57.5 \pm 0.5$. Three observations support this result: (i) the change of the distance dependence of $G_6(r)$ (Fig. 4), (ii) the condition $F_A(\Gamma_i) = 72/\pi$ for Frank's constant, and (iii) the divergence of ξ_6. For the transition hexatic $\leftrightarrow$ crystal F_A diverges at Γ_m. Both divergencies (extracted from just one correlation function) are in agreement with the KTHNY theory. The measurements for melting and freezing support each other, so we may conclude that there is no hysteresis effect of the phase transitions. At the two transitions, the order parameters are observed to change continuously (within the resolution of $\Gamma \propto 1/T$) and no indication of a phase separation (like strong fluctuations of the order parameters or heterogeneous probability distributions of the local bond-order parameter) has been found [32]. So we believe that in our system—having a well-defined, purely
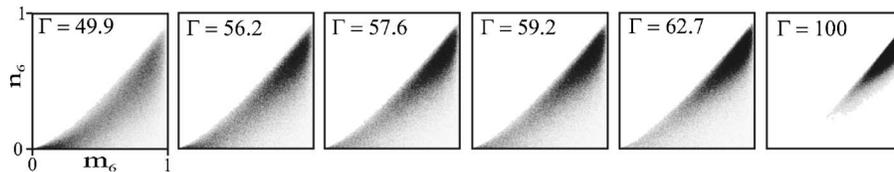

FIG. 7. Gray-scale image (a.u.) of the probability distribution of the magnitude of the local bond-order parameter m_6 versus the magnitude of the projection of m_6 to the mean of nearest neighbors n_6 for the same temperatures as in Fig. 6. The probability distribution changes continuously at both phase transitions and no bimodal distribution can be found.

repulsive pair potential and a confinement to 2D that is free of any surface roughness—the transitions are second order.

In [33,34] we showed that the Young's modulus becomes 16π at T_m, implying that the dislocation unbinding condition is satisfied at T_m. We also showed that the softening is indeed due to the dislocation pairs in the crystalline phase and that this softening is well described by the renormalization equations of Halperin, Nelson, and Young. But this alone does not suffice to rule out an alternative melting scenario [6,7] where dislocations arrange themselves in grain boundaries, destroying the orientational symmetry before a disclination unbinding appears. We have now completed the picture by checking the disclination unbinding condition. We indeed found that F_A takes the value $72/\pi$ at T_i. This now fully confirms the microscopic scenario of Halperin and Nelson and suggests that the orientational symmetry changes at T_i because of disclination-pair unbinding.

ACKNOWLEDGMENT

[1] N. D. Mermin, Phys. Rev. **176**, 250 (1968).

[2] J. Kosterlitz and D. Thouless, J. Phys. C **6**, 1181 (1973).

[3] A. P. Young, Phys. Rev. B **19**, 1855 (1979).

[4] B. I. Halperin and D. R. Nelson, Phys. Rev. Lett. **41**, 121 (1978).

[5] D. R. Nelson and B. I. Halperin, Phys. Rev. B **19**, 2457 (1979).

[6] S. T. Chui, Phys. Rev. B **28**, 178 (1983).

[7] H. Kleinert, Phys. Lett. **95A**, 381 (1983).

[8] M. A. Glaser and N. A. Clark, Adv. Chem. Phys. **83**, 543 (1993).

[9] Y. Lansac, M. A. Glaser, and N. A. Clark, Phys. Rev. E **73**, 041501 (2006).

[10] K. Chen, T. Kaplan, and M. Mostoller, Phys. Rev. Lett. **74**, 4019 (1995).

[11] F. L. Somer, G. S. Canright, T. Kaplan, K. Chen, and M. Mostoller, Phys. Rev. Lett. **79**, 3431 (1997).

[12] A. Jaster, Phys. Rev. E **59**, 2594 (1999).

[13] C. H. Mak, Phys. Rev. E **73**, 065104(R) (2006).

[14] S. Z. Lin, B. Zheng, and S. Trimper, Phys. Rev. E **73**, 066106 (2006).

[15] C. A. Murray and D. H. Van Winkle, Phys. Rev. Lett. **58**, 1200 (1987).

[16] Y. Tang, A. J. Armstrong, R. C. Mockler, and W. J. O'Sullivan, Phys. Rev. Lett. **62**, 2401 (1989).

[17] R. E. Kusner, J. A. Mann, J. Kerins, and A. J. Dahm, Phys. Rev. Lett. **73**, 3113 (1994).

[18] A. H. Marcus and S. A. Rice, Phys. Rev. Lett. **77**, 2577 (1996).

[19] K. Zahn and G. Maret, Phys. Rev. Lett. **85**, 3656 (2000).

[20] A. V. Petukhov, D. van der Beek, R. P. A. Dullens, I. P. Dolbnya, G. J. Vroege, and H. N. W. Lekkerkerker, Phys. Rev. Lett. **95**, 077801 (2005).

[21] R. A. Segalman, A. Hexemer, R. C. Hayward, and E. J. Kramer, Macromolecules **36**, 3272 (2003).

[22] D. E. Angelescu, C. K. Harrison, M. L. Trawick, R. A. Register, and P. M. Chaikin, Phys. Rev. Lett. **95**, 025702 (2005).

[23] R. Seshadri and R. M. Westervelt, Phys. Rev. B **46**, 5142 (1992).

[24] P. M. Reis, R. A. Ingale, and M. D. Shattuck, Phys. Rev. Lett. **96**, 258001 (2006).

[25] X. H. Zheng and R. Grieve, Phys. Rev. B **73**, 064205 (2006).

[26] P. Dimon, P. M. Horn, M. Sutton, R. J. Birgeneau, and D. E. Moncton, Phys. Rev. B **31**, 437 (1985).

[27] D. Li and S. A. Rice, Phys. Rev. E **72**, 041506 (2005).

[28] P. Keim, G. Maret, U. Herz, and H. H. von Grünberg, Phys. Rev. Lett. **92**, 215504 (2004).

[29] The segments will merge to rings if the system's size tends towards infinity.

[30] The upper value is motivated by the maximum value of the histogram of distances and $r/a=0$ is excluded in the algebraic case to avoid the singularity. The histogram over distances is used as statistical weight of the fit function taking into account the different frequency of occurrence of the data points in the minima and maxima of $G_6(r)$.

[31] A. E. Larsen and D. G. Grier, Phys. Rev. Lett. **76**, 3862 (1996).

[32] We indeed do see a local clustering of dislocations as already noted by [15,16] in the hexatic phase close to Γ_i (which is not too surprising for dislocations with finite density having an attractive interaction) but this averages out in G_6 if the field of view is big enough.

[33] H. H. von Grünberg, P. Keim, K. Zahn, and G. Maret, Phys. Rev. Lett. **93**, 255703 (2004).

[34] J. Zanghellini, P. Keim, and H. H. von Grünberg, J. Phys.: Condens. Matter **17**, 3579 (2005).